SARS-CoV-2 infection in the central nervous system of a 1-year-old infant

Ismael Gomes, BSc [1,3]*, Karina Karmirian, BSc [2,3]*, Júlia T. Oliveira, PhD [2]*, Carolina da S. G. Pedrosa, PhD [2]*, Mayara Abud Mendes, PhD [2], Fernando Colonna Rosman, MD [1,5], Leila Chimelli, MD [4]#, Stevens Rehen, PhD [2,3]#

*These authors contributed equally to this work

#Co-senior authorship

Corresponding author:

Stevens Rehen (srehen@lance-ufrj.org)

+55 21 38836000

Affiliation details:

1 - Anatomic Pathology Service, Jesus Municipal Hospital, Rio de Janeiro, RJ, Brazil.

2 – D'Or Institute for Research and Education (IDOR), Rio de Janeiro, Brazil.

3 – Institute of Biomedical Sciences, Federal University of Rio de Janeiro (UFRJ), Rio de Janeiro, Brazil.

4 - Laboratory of Neuropathology, State Institute of Brain Paulo Niemeyer, Post-Graduate Programs of Pathology and Translational Neuroscience, UFRJ, Rio de Janeiro, RJ, Brazil.

5 - Department of Pathology, School of Medicine, UFRJ, Rio de Janeiro, Brazil.

We report the case of a female 1-year-old infant who died twenty-five days after hospitalization, due to respiratory failure caused by bilateral coronavirus pneumonitis. She was admitted to the hospital presenting vomits and repetitive movements in the left upper and lower limbs, hypotonia, postural instability, inability to support her head, to sit and walk. The auscultation of the respiratory system revealed universally audible vesicular murmur, wheezing, rhonchi, and rales. She evolved with intermittent periods of dyspnea, tachypnea, and use of accessory muscles to breathe, along with tachycardia (154 bpm), fever, anemia, leukocytosis (30-35x10^3 cells/uL), relative lymphopenia, and neutrophilia. She also presented elevated alanine aminotransferase, aspartate aminotransferase and C-reactive protein levels, normal bilirubin values, and metabolic acidosis. Oxygen therapy and assisted ventilation were required due to the respiratory alkalosis and severe hypoxemia (79-88% SpO2). The tracheal secretion tested positive for SARS-CoV-2 by RT-qPCR, and the cranial computed tomography showed brain atrophy with compensatory hydrocephalus. She evolved to impaired consciousness (Glasgow scale 3) and hemodynamic instability, followed by death by respiratory failure. The laboratory parameters evaluated during hospitalization are listed in Table 1.

A full autopsy was performed revealing damages in multiple organs, including venous and arterial microthrombosis in several regions (supplementary figure 1). A full description of other morphological findings was reported in supplementary table 1 and supplementary figure 2. As expected, coronavirus pneumonitis caused lung congestion and edema; the interstitial inflammation delineated the pulmonary acini (figure 1A). Histologically, it was characterized by some bronchial lymphoid aggregates, interstitial lymphocytic infiltrate, and diffuse damage of respiratory bronchioles covered with hyaline membranes, along with collapsed alveolar space, some of them containing eosinophilic plugs of plasma proteins and cellular debris (figure 1B, C). In addition, we found congestion, edema, hemorrhagic foci, atelectasis, and recent microthrombi in some branches of pulmonary arteries in both lungs (supplementary figure 1A).

A comprehensive analysis of the brain showed severe cerebral atrophy with a large remaining space within the cranial cavity (figure 1D). The brain weight (635 grams) was about 33% less than normal parameters for the age (range weight: 940 to 1,010 grams). Indeed, we observed a significant atrophy on sections of the cerebral hemispheres, the cortical surfaces were thin, granulated and discolored (supplementary figure 3A), and there were focal cortical depressions corresponding to areas of cortical

collapse, particularly in the temporal lobes, which were extremely soft. The cerebellum looked normal but the basis pontis was smaller than the expected average for this age group. The olfactory nerves and bulbs were not preserved because of the cerebral softening.

Also, we observed pronounced damage in many regions of the cerebral cortex, such as laminar cortical necrosis, spongiosis, microvascular proliferation, and diffuse cerebral edema (figure 1E, F). Pannecrotic cortical lesions featured profound neuronal loss particularly in the temporal lobes. Additionally, we observed neuronal loss in the basal ganglia and the thalamus. The appearances were consistent with anoxic encephalopathy. White matter myelination was preserved (supplementary figure 3B). The cerebellum was relatively preserved with occasional red or shrunken Purkinje cells which were scarcer in some regions. The brainstem presented few descending axons. Severe loss of cortical neurons was highlighted with immunostaining for NeuN (figure 1G). We also noticed a severe reactive gliosis involving basal ganglia and the periventricular region (figure 1H), and microglial/macrophagic proliferation (figure 1I).

In order to investigate SARS-CoV-2 infection, we analyzed the lung and, as expected, SARS-CoV-2 was present in groups of nearby cells in the parenchyma, which was detected by immunostaining for Spike protein (SP) (figure 2A-C). In the brain, we observed a pronounced SARS-CoV-2 staining localized along the apical region of the choroid plexus (ChP) epithelium (figure 2D-F). Considering that ChP extends within each ventricle in the brain, not surprisingly, we also detected SARS-CoV-2 positive cells, to a lesser extent, in the ependyma of the lateral ventricle (figure 2G-I). We also observed scarce positive cells for SP in the cortex (figure 2J-L), whereas no positive cells were found in the medulla oblongata, pons, midbrain, and putamen, neither in control samples from non-COVID-19 patients (supplementary figure 4). SARS-CoV-2 infection was further confirmed by nucleocapsid proteins N1 and N2 detection by RT-qPCR in distinct fragments from lung, choroid plexus, lateral ventricle, and cortex (figure 2M). We also demonstrated, for the first time in an infant, the presence of SARS-CoV-2 protein fragments in a wide variety of other tissue samples such as heart, kidney, liver, stomach, trachea, larynx, cerebellum (supplementary table 2).

We found SARS-CoV-2 infection restricted at the lumina of some ChP capillaries and vessels, which was detected by immunostaining for double-stranded RNA (dsRNA)

(figure 3A-C), convalescent serum of a patient recovered from COVID-19 (CS) (figure 3D-F), and SP (figure 3G-I). Some vessels of the ChP presented the entire wall infected by SARS-CoV-2 (supplementary figure 5E, F), whereas in other vessels, the group of cells next to the infected endothelium presented higher immunoreactivity to SARS-CoV-2 than cells alongside the vessel wall (figure 3A and C, supplementary figure 5B, C and E), which suggests the course of virus spreading in the brain.

In this work, we demonstrated that SARS-CoV-2 substantially infected the ChP epithelium and endothelium, some ependymal cells and in a lesser extension the cerebral cortex. This is the first evidence of SARS-CoV-2 infection in the central nervous system of an infant who died of COVID-19.

The brain presents negligible amounts of ACE2 protein, with ChP exhibiting the highest expression of ACE2 (1,2). Indeed, we found substantial immunostaining for SARS-CoV-2 in ChP and, to a lesser extent, in ependymal cells, but it was scarce in other brain areas, such as the cortex. These findings are in accordance with previous works *in vitro* showing SARS-CoV-2 infection in human ChP organoids (3,4). The authors demonstrated that SARS-CoV-2 has minimal tropism for neurons and glial cells but promotes the brain-CSF barrier breakdown (4).

ChP has a single epithelial layer attached by tight junctions that participates in the blood-cerebrospinal fluid (CSF) barrier (5–7). A study evidenced SARS-CoV-2 particles in endothelial cells, as well as inflammation (8). Another study found viral-like particles in brain capillary endothelium, suggesting the hematogenous route as the most likely pathway for SARS-CoV-2 to the brain (9). Given the essential role of endothelium in vascular permeability homeostasis, endothelium dysfunction caused by SARS-CoV-2 infection may contribute to the thromboinflammatory process resulting in vasculopathy (10). Thus, infection of the ChP by SARS-CoV-2 could enable it to disrupt the CSF barrier and invade the brain. Supporting this concept, SARS-CoV-2 RNA was found in the cerebrospinal fluid of one patient with COVID-19 encephalitis (11) and SARS-CoV-2 nucleocapsid protein (N) genes were also detected in the ChP, as we demonstrated here.

In summary, we reported multisystemic histopathological alterations caused by SARS-CoV-2 in an infant. Corroborating with previous studies, our findings suggest that SARS-CoV-2 neuroinvasion may occur via blood-CSF barrier disruption. Although we

did not observe effective SARS-CoV-2 spreading within the brain parenchyma, the excessive microgliosis, unusual in cases of anoxic encephalopathy, but frequently associated with viral infections (12), showed that the infection might be profoundly harmful. The differences in SARS-CoV-2 behavior between infants/children and adults are not clear, but they seem to share critical hallmarks, including inflammation, thrombosis, and secondary tissue hypoxia (13–16). Despite the rarity of the severe SARS-CoV-2 cases in infants/children, they may lead to death or sequelae in many cases, becoming an important public health issue (17). This case report helps to elucidate aspects of SARS-CoV-2 infection in the brain and could shed light on COVID-19 outcomes in infants.

Acknowledgements

We thank Leticia Souza for technical support in confocal images acquisition; Diego Santos and Heliomar Pereira Marcos for immunohistochemical staining technique. Financial support (not specifically for COVID-19 studies) was provided by the Foundation for Research Support in the State of Rio de Janeiro (FAPERJ); the National Council of Scientific and Technological Development (CNPq) and Coordination for the Improvement of Higher Education Personnel (CAPES), in addition to intramural grants from D'Or Institute for Research and Education.

Author contributions

ICG, FCR and SR conceptualized the study. FCR performed the autopsy and full histological analysis. LC performed the neuropathological analysis. ICG performed material preparation for histological procedures and immunofluorescence stainings. ICG, KK and CSGP performed confocal images analysis. MAM performed RNA isolation and RT-qPCR for viral detection in human *postmortem* tissues. KK and LC prepared the figure panels. The first draft of the manuscript was written by KK, JTO and CSGP. All authors discussed the results and contributed to the final version of the manuscript. All authors read and approved the final manuscript. LC and SR coordinated the study.

Ethical Statement

The research protocol was approved by the local Ethics Committee (Copa D'Or Hospital/Instituto D'Or de Pesquisa e Ensino, IDOR, CAAE number: 37211220.0.0000.5249), and was performed according to the Declaration of Helsinki. The use of the convalescent serum from COVID-19 patients was approved by CAAE number: 30650420.4.1001.0008.

Competing interests

The authors declare no competing interests.

References:

1. Hikmet F, Méar L, Edvinsson Å, Micke P, Uhlén M, Lindskog C. The protein expression profile of ACE2 in human tissues. Mol Syst Biol. 2020;
2. Chen R, Wang K, Yu J, Howard D, French L, Chen Z, et al. The spatial and cell-type distribution of SARS-CoV-2 receptor ACE2 in human and mouse brain. bioRxiv [Internet]. 2020 Jan 1;2020.04.07.030650. Available from: http://biorxiv.org/content/early/2020/06/15/2020.04.07.030650.abstract
3. Jacob F, Pather SR, Huang WK, Zhang F, Wong SZH, Zhou H, et al. Human Pluripotent Stem Cell-Derived Neural Cells and Brain Organoids Reveal SARS-CoV-2 Neurotropism Predominates in Choroid Plexus Epithelium. Cell Stem Cell. 2020;
4. Pellegrini L, Albecka A, Mallery DL, Kellner MJ, Paul D, Carter AP, et al. SARS-CoV-2 Infects the Brain Choroid Plexus and Disrupts the Blood-CSF Barrier in Human Brain Organoids. Cell Stem Cell. 2020;
5. Brightman MW. The Intracerebral Movement of Proteins Injected into Blood and Cerebrospinal Fluid of Mice. Prog Brain Res. 1968;
6. Milhorat TH, Davis DA, Lloyd BJ. Two morphologically distinct blood-brain barriers preventing entry of cytochrome c into cerebrospinal fluid. Science (80-).

1973;

7. Lun MP, Monuki ES, Lehtinen MK. Development and functions of the choroid plexus-cerebrospinal fluid system. Nature Reviews Neuroscience. 2015.

8. Varga Z, Flammer AJ, Steiger P, Haberecker M, Andermatt R, Zinkernagel AS, et al. Endothelial cell infection and endotheliitis in COVID-19. The Lancet. 2020.

9. Paniz-Mondolfi A, Bryce C, Grimes Z, Gordon RE, Reidy J, Lednicky J, et al. Central nervous system involvement by severe acute respiratory syndrome coronavirus-2 (SARS-CoV-2). Journal of Medical Virology. 2020.

10. McGonagle D, O'Donnell JS, Sharif K, Emery P, Bridgewood C. Immune mechanisms of pulmonary intravascular coagulopathy in COVID-19 pneumonia. The Lancet Rheumatology. 2020.

11. Moriguchi T, Harii N, Goto J, Harada D, Sugawara H, Takamino J, et al. A first case of meningitis/encephalitis associated with SARS-Coronavirus-2. Int J Infect Dis. 2020;

12. Ellison D, Love S, Chimelli L, Harding B, Lowe J, Vinters H V., et al. Neuropathology. A Reference Text of CNS Pathology. 3th Edition. London: Elsevier; 2013.

13. Lazzaroni MG, Piantoni S, Masneri S, Garrafa E, Martini G, Tincani A, et al. Coagulation dysfunction in COVID-19: The interplay between inflammation, viral infection and the coagulation system. Blood Reviews. 2020.

14. Pedersen SF, Ho YC. SARS-CoV-2: A storm is raging. Journal of Clinical Investigation. 2020.

15. Riphagen S, Gomez X, Gonzalez-Martinez C, Wilkinson N, Theocharis P. Hyperinflammatory shock in children during COVID-19 pandemic. The Lancet. 2020.

16. Yuki K, Fujiogi M, Koutsogiannaki S. COVID-19 pathophysiology: A review. Clinical Immunology. 2020.

17. Stafstrom CE, Jantzie LL. COVID-19: Neurological Considerations in Neonates and Children. Children. 2020;

18. Pires ARC, Da Matta Andreiuolo F, De Souza SR. TMA for all: A new method for the construction of tissue microarrays without recipient paraffin block using custom-built needles. Diagn Pathol. 2006;

19. Winther L, Lohse J, Gabs S, Petersen K. Immunohistochemistry Detection Method [Internet]. 2007. Available from: http://patentscope.wipo.int/search/en/WO2007023390. Accessed August 3, 2020.

Table 1: Patient's laboratory parameters at different timepoints post admission

Laboratory parameters	Days post admission						Normal range
	4	10	14	17	23	25	
Haemoglobin, g/dL	16·6	12·3	12·3	9·9	10·1	10·6	12·6 ± 1.5
Hematocrit, %	48·5	35·6	35·9	··	29·6	32	34 ± 4
Platelets, ×10^3 cells/µL	304	··	343	295	383	393	200 - 550
Erythrocytes, x10^6/uL	5·7	4·25	··	··	··	··	4·04 - 6·13
Leukocytes, ×10^3 cells/µL	15·7	20·2	32·7	17·5	24·6	35·8	6 - 16
Lymphocytes, %	41	18	10	16	20	13	10 - 50
Segmented neutrophils, %	43	48	73	75	67	58	37 - 80
Band neutrophils, U/µL	3	1	4	2	7	25	300
Alkaline phosphatase, U/L	··	1171	··	928	··	1086	65 - 645
Creatinine, mg/dL	0.4	0·4	0·3	0·3	0·3	0·3	0·3 – 0·8
Urea, mg/dL	25	14	27	22	13	17	10 - 50
C-reactive protein, mg/L	2	0·8	6·1	26·7	108·1	··	0 - 5
Aspartate aminotransferase, U/L	131	78	69	175	106	114	0 - 38
Alanine aminotransferase, U/L	47	71	82	197	100	129	0 - 42
Total bilirubin, mg/dL	··	0·11	··	··	··	0·18	0·2 - 1

Figures and Legends:

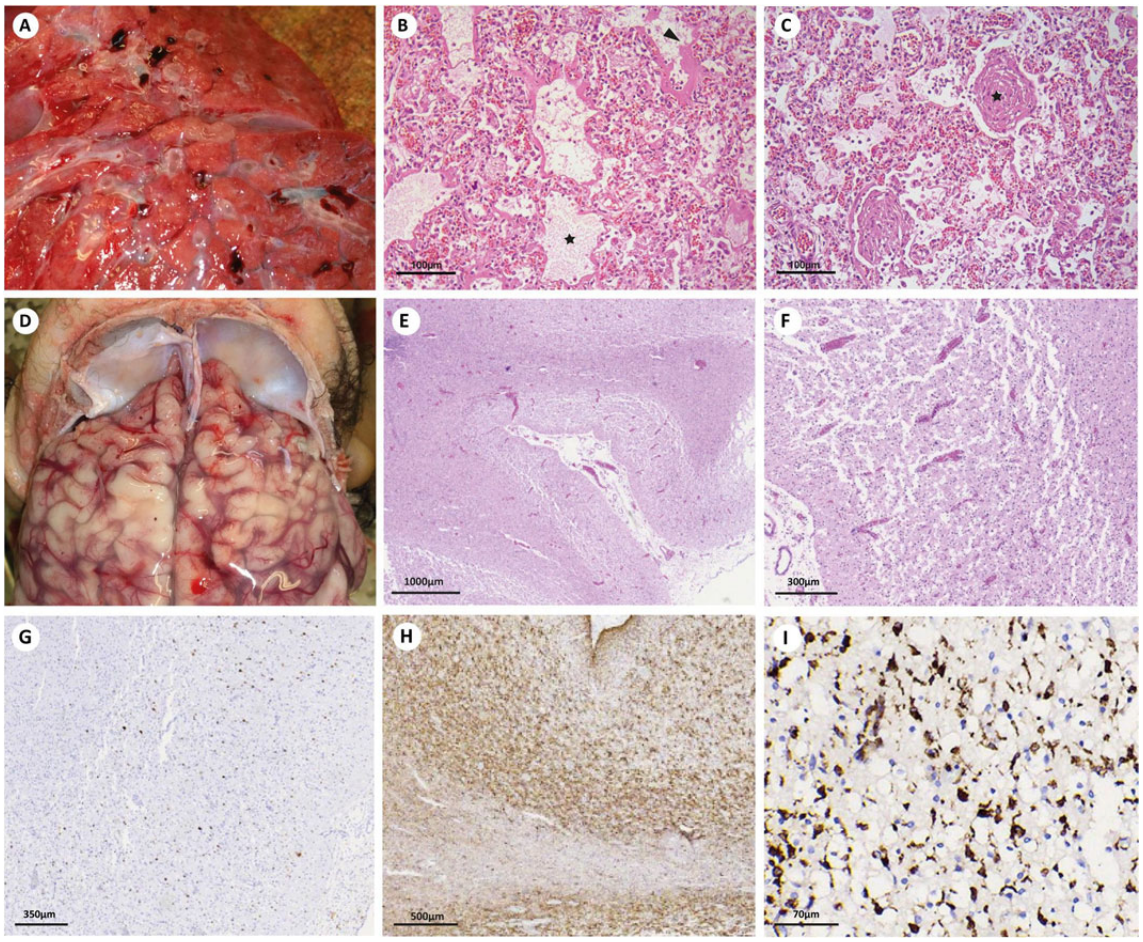

Figure 1 **Macroscopic and microscopic appearance of lungs and brain tissue** **(A)** Cut surface of congested and edematous lungs. The pulmonary acini (lobules) are well delimited due to the pneumonitis. *Post-mortem* clots are seen in branches of pulmonary arteries. **(B)** Diffuse damage of respiratory bronchioles (star) associated with eosinophilic hyaline membranes (arrowhead). Note the congestion of the alveolar capillaries, the collapsed alveolar spaces and the interstitial lymphocytic infiltrate. Scale bar: 100 µm. **(C)** Respiratory bronchioles with eosinophilic plugs (star) of plasma proteins and cellular debris. Observe the collapsed alveolar spaces and some hyaline membranes. Scale bar: 100 µm. **(D)** Unfixed brain in situ does not fill the base of the skull due to marked atrophy. **(E)** Histological section of cortex and white matter, showing cortical laminar necrosis. Scale bar: 1000 µm. Detail in **(F)** Scale bar: 300 µm. There is severe nerve cell loss and vascular proliferation, but the molecular layer (left) is relatively spared. **(G)** Immunostaining for NeuN demonstrating severe cortical nerve cell loss. Scale bar: 350 µm. **(H)** Immunostaining for GFAP revealing severe reactive gliosis involving cortex and white matter. Scale bar: 500 µm. **(I)** Immunostaining for CD68 exhibiting microglial and macrophagic proliferation in cortex and white matter. Scale bar: 70 µm.

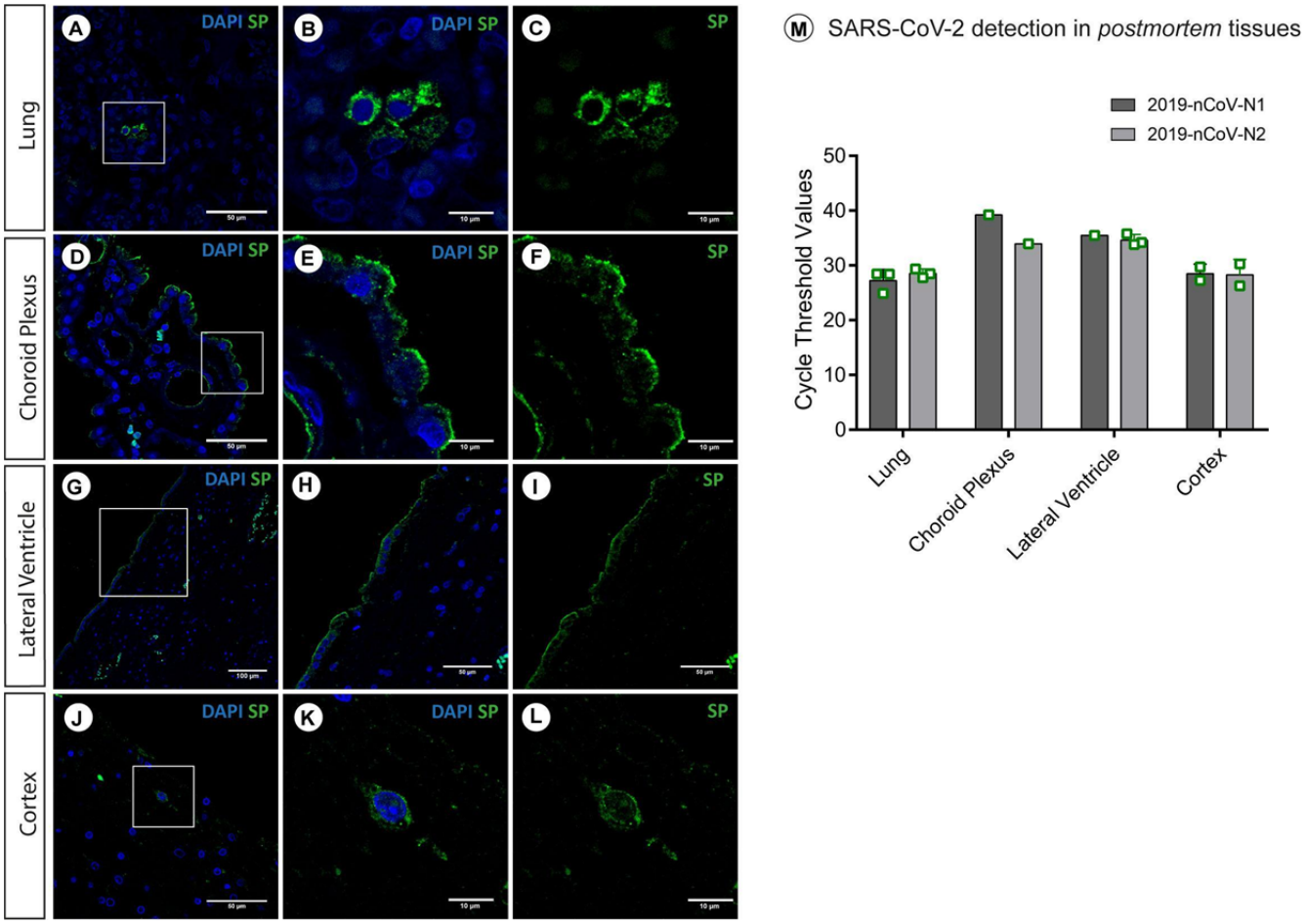

Figure 2 **SARS-CoV-2 detection in lungs, choroid plexus, lateral ventricle and cerebral cortex.** Photomicrographs of immunostaining for spike protein (SP) in lung tissue **(A-C)** and in the brain (choroid plexus - **D-F**; lateral ventricle - **G-I**; cerebral cortex - **J-L**). Scale bars: (A, D, H, I, J) 50 µm; (G) 100 µm; (B, C, E, F, K, L) 10 µm. **(M)** RT-qPCR detection of SARS-CoV-2 regions of nucleocapsid (N) genes (N1 and N2). Data are mean ± SD. Each square indicates the cycle threshold values of a distinct fragment from the same *postmortem* specimen of lung (n = 3), choroid plexus (n = 1), lateral ventricle (n = 3), cortex (n = 2). The complete panel of SARS-CoV-2 detection in infant tissue samples is demonstrated in the **Supplementary Table 2**.

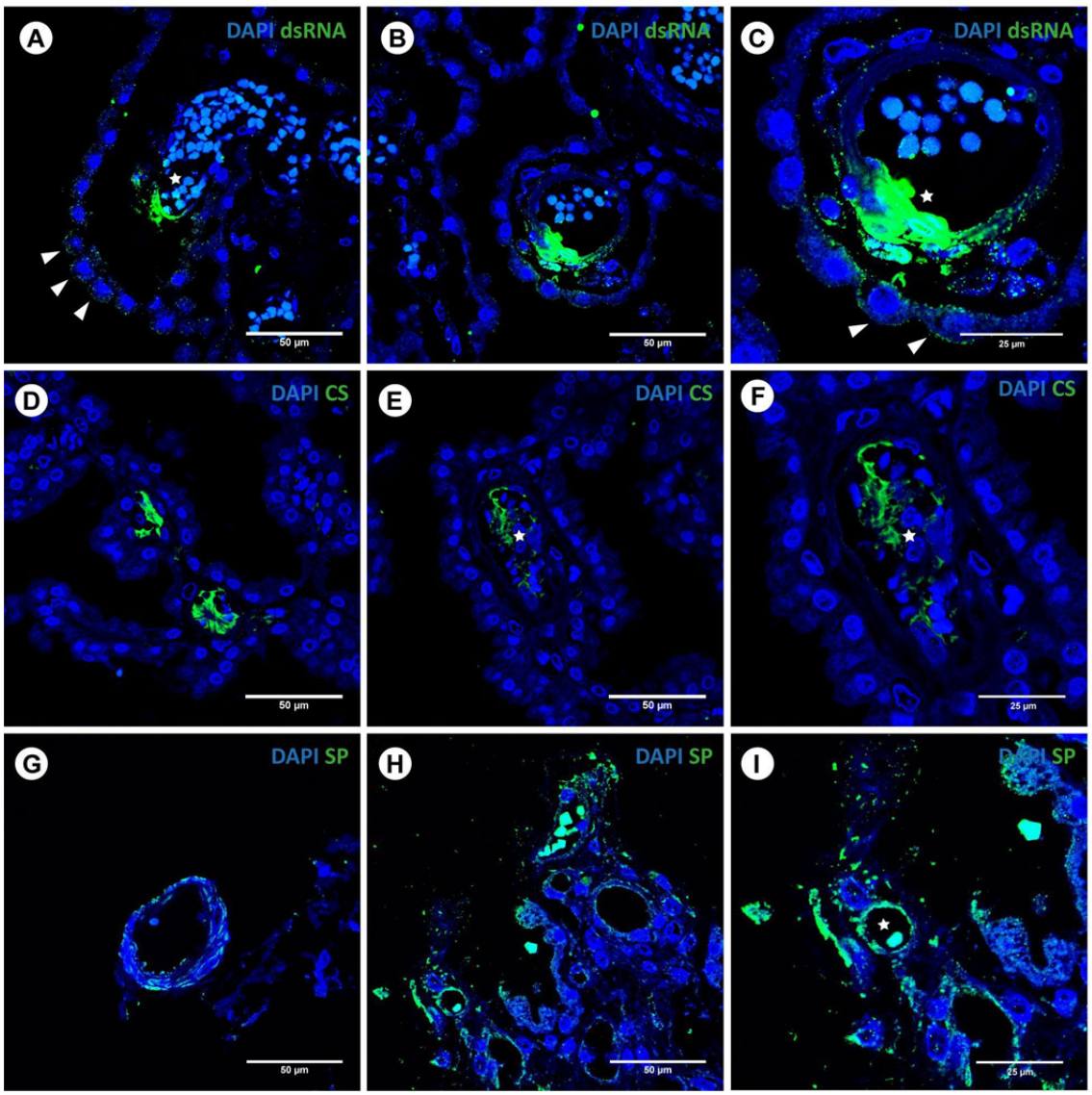

Figure 3 **Photomicrographs of immunostaining for SARS-CoV-2 in the choroid plexus endothelium**. dsRNA (A-C), CS (D-F) and spike protein (SP) (G-I) stainings in green and nuclear staining in blue (DAPI). SARS-CoV-2 infection at the lumina of capillaries and vessels (stars) and nearby cells infected (arrowheads). Scale bars: 50 µm. Details in (C), (F) and (I); Scale bars: 25 µm.